Available online at www.sciencedirect.com
ScienceDirect
Materials Chemistry and Physics 101 (2007) 433–440
MATERIALS CHEMISTRY AND PHYSICS
www.elsevier.com/locate/matchemphys

Synthesis of SnO_2 nanoparticles through the controlled precipitation route

C. Ararat Ibarguen [a,*], A. Mosquera [a], R. Parra [b,*], M.S. Castro [b], J.E. Rodríguez-Páez [a]

[a] Grupo de Ciencia y Tecnología de Materiales Cerámicos, CYTEMAC, Universidad del Cauca, Calle 5 No. 4-70 Popayán, Cauca, Colombia
[b] Instituto de Investigaciones en Ciencia y Tecnología de Materiales (INTEMA, CONICET-UNMdP) J.B. Justo 4302, B7608FDQ Mar del Plata, Argentina

Received 17 February 2006; accepted 24 August 2006

Abstract

The controlled precipitation method allowed to the synthesis of SnO_2 with advantageous specific properties, such as size and shape employing an aqueous $SnCl_2{\cdot}2H_2O$ solution as precursor. Through XRD analyses, the optimum pH value of the solution that yielded the desired product was found to be 6.25. After a thermal treatment at 600 °C, the final powder presented an average particle size below 50 nm with a surface area of 19 $m^2\ g^{-1}$ and a large reactivity. The evolution of the most important functional groups during the steps involved in this synthesis route is explained in view of the results obtained with FTIR and XRD. A thorough discussion on the different intermediates involved in the whole process is presented on the basis of hydrolysis and condensation reactions. The conclusions are supported with a complete characterization through differential and gravimetric thermal analysis (DTA/TGA), electron microscopies (SEM/TEM) and surface area determinations (BET).

Keywords: Powders; Chemical preparation; Nanoparticles; Tin oxide; Controlled precipitation

1. Introduction

The synthesis of nanoparticles has become a highly developed field owing to the scientific and technological interest due to the structural peculiarities and unusual physical and chemical properties they may lead to [1,2]. Nano-scaled particles are of great importance if the conformation of ceramics is considered; they have been found to enhance the mechanical, electrical, thermal, catalytic and optical properties of diverse ceramic materials [3,4]. The specific advantages of these nanocrystallised materials lie in the high homogeneity attained and in the possibility of sintering at lower temperatures. The crystalline structure, the size and shape of the particles and the superficial characteristics are highly dependent on the followed route of synthesis. Then, it is necessary to adjust the synthesis methods of nanoparticles to assure the high quality of the ceramic powder; properties related to size uniformity, particle morphology, purity and chemical homogeneity are critical during the processing and sintering steps of the compacted powder and determine the microstructure of the ceramic and the final properties of the resulting piece. A brief description of the synthesis route is no longer satisfactory; there exists an urge to know the basic physicochemical processes that occur during the formation of the nanoparticles. This would provide an aid in establishing the mechanisms of particle formation and would also be of importance in controlling the final properties of the ceramic powder obtained [5,6].

Tin dioxide (SnO_2), with a rutile-type crystalline structure, is an n-type wide band gap (3.5 eV) semiconductor that presents a proper combination of chemical, electronic and optical properties that make it advantageous in several applications [7]. Due to its physical properties, such as transparency and semiconductivity, it is an oxide of great interest from the technological point of view for gas sensors [8], white pigments for conducting coatings, transparent conducting coatings for furnaces and electrodes [9], opto-conducting coatings for solar cells [10], catalysts [11,12] and surge arrestors (varistors) [13,14]; an increasing interest in the use of anodes of SnO_2 in lithium batteries has been recently noticed [15].

Nanoparticles of tin dioxide have been synthesized through different chemical routes, such as precipitation [15,16], hydrothermal [8,17], sol–gel [18,19], hydrolytic [20], carbothermal reduction [21] and polymeric precursor [22] methods among others. Even though the development of agglomerates is to be avoided, their growing is somehow inevitable due to the small diameter of the oxide particles and to the presence of the compounds involved in the mentioned procedures, mainly solvents. On the other hand, the most used tin precursors are

* Corresponding authors. Tel.: 54 2234816600; fax: 54 2234810046.
E-mail addresses: cararat@unicauca.edu.co (C.A. Ibarguen), rparra@fi.mdp.edu.ar (R. Parra).

0254-0584/$ – see front matter © 2006 Published by Elsevier B.V.
doi:10.1016/j.matchemphys.2006.08.003

tin chlorides ($SnCl_2$ or $SnCl_4$) provided their low cost and their easy handling characteristics; however, the chlorine ion is difficult to remove from the system and it seriously alters the superficial and electrical properties of the material modifying, for instance, the sensibility of the gas sensor [23], favouring the agglomeration of particles [24] and leading to higher sintering temperatures [25]. The chloride problem can be avoided through the usage of organic tin compounds, such as alkoxides. However, these reagents are rather costly which makes the industrial synthesis implementation hardly attainable.

In this work, the synthesis of tin dioxide nanoparticles through the controlled precipitation method is described. On the basis of potentiometric and conductimetric titrations, the reaction of the system to the precipitant (ammonium hydroxide) addition and the evolution of the process in different stages are discussed. The main physicochemical phenomena that take place are addressed and a detailed description of the critical steps to eliminate chloride ions and to reduce the nanoparticle agglomeration is also given in this paper.

2. Experimental procedure

2.1. Pontentiometric titration

Potentiometric titration curves of aqueous dissolutions of $SnCl_2{\cdot}2H_2O$ (Mallinckrodt) 0.01, 0.1 and 0.3 M were obtained through the addition of 0.5 ml every 15 s of a 28 wt% solution of ammonium hydroxide (NH_4OH, Merck) with a Metrohm Dosimat 685 dosimeter. The pH evolution was recorded with a Metrohm 744 pH-meter working with a glass electrode previously calibrated with buffer solutions of pH 4 and 7. Distilled and deionised water was used for the $SnCl_2{\cdot}2H_2O$ dissolution, which was kept in continuous stirring for a reasonable time as to assure the complete dissolution of the salt. The pH value of the system, as well as the volume of base added, was registered periodically during the addition of NH_4OH until pH 10 was reached.

2.2. Conductimetric titration

Simultaneously to the recording of the pH variation in the system, changes in the specific conductivity of the solution were measured with a Metrohm 712 conductimeter. The specific conductivity was also studied as function of the volume of base added until pH 10 was reached.

2.3. Synthesis of SnO_2 nanoparticles through the controlled precipitation route

The optimal pH value to obtain SnO_2 nanoparticles was determined after the titration curves that contain the information of the evolution of the process and of the physicochemical phenomena that take place during the addition of the hydroxide. The dissolution was taken to the pH value of interest and the obtained colloidal suspension was filtered and subjected to a series of washings with 0.05 M diethylamine solution to eliminate chloride ions. Before each filtering step, the pH of the suspension was adjusted to the desired value through drop wise addition of HNO_3. Afterwards, the system was dispersed and homogenized with an Ultra-turrax T50 turbine and aged during 24 h. Finally, the suspension was filtered in vacuum and dried at 60 °C during 12 h for the subsequent thermal treatments.

2.4. Characterization of powders

The ceramic powders were characterized with X-ray diffraction (XRD) with a Rigaku 2200 equipment running with Cu Kα radiation in the range of 20–70° (2θ). Simultaneous gravimetric and differential thermal analyses (TGA/DTA) were carried out in synthetic air flux with heating rates of 5 °C min^{-1} in a Shimadzu TGA-50 and in a Shimadzu DTA-50, respectively. Infrared spectra were registered in absorbance mode with a Nicolet IR 200 FTIR spectrometer at room temperature. Surface area measurements (BET) were made with an SE Micromeritics ASAP 2010. The morphology and size of the particles obtained were examined with transmission electron microscopy (TEM) by means of a JEOL 1200 EX microscope and with scanning electron microscopy (SEM) by means of Topcon SM 300. Sample preparation for microscopy consisted in the deposition of small drops of a dispersion of the powder in ethanol onto usual copper grids.

3. Results and discussion

3.1. Titration curves: tin hydrolysis and condensation reactions

Potentiometric and conductimetric titration curves of the 0.3 M $SnCl_2$ dissolution are shown in Fig. 1. Four regions can be clearly distinguished in the potentiometric titration curve; two steps (pH AB and CD) and two plateaus (pH BC and DE).

During the dissolution of the tin(II) chloride, before the addition of the ammonium hydroxide solution, the pH drops below 2 indicating that the concentration of H^+ species is increasing. This could be originated by the difficult dissociation of $SnCl_2$

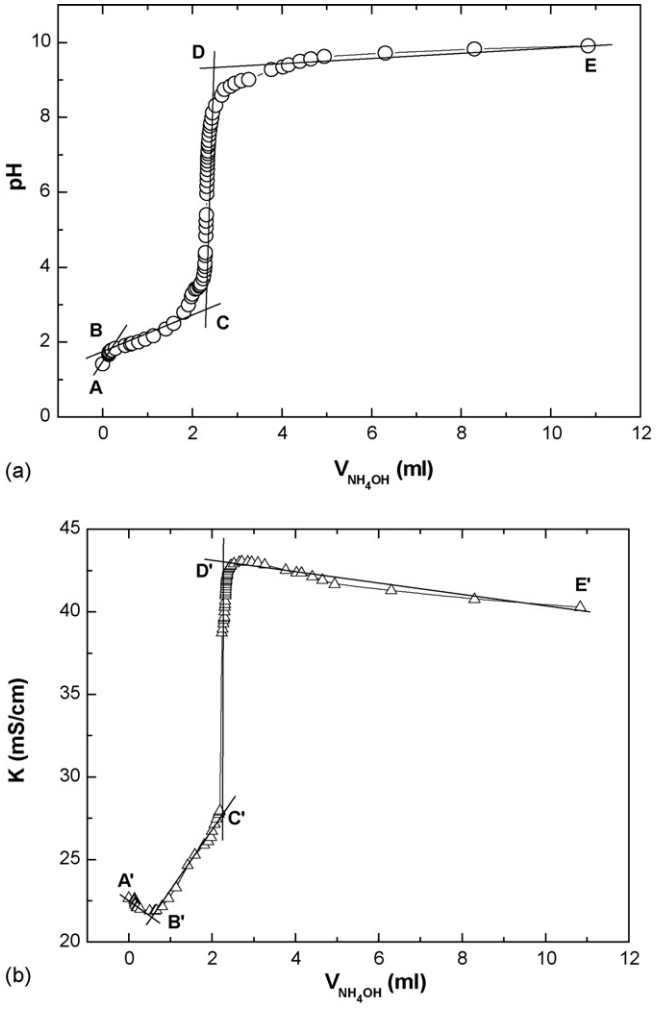

Fig. 1. (a) Potentiometric and (b) conductimetric titration curves of a 0.3 M $SnCl_2$ aqueous dissolution.

in the solvent that leads to the formation of a basic chloride tin complex according to the following reaction [26]:

$$SnCl_2 + H_2O \rightarrow SnCl(OH) + Cl^- + H^+. \quad (1)$$

At low pH values, pH < 2, the Sn^{2+} acid cation present in the medium hydrolyses easily into the following species [27]:

$$Sn^{2+} + H_2O \rightleftarrows Sn(OH)^+ + H^+, \quad (2)$$

$$2Sn^{2+} + 2H_2O \rightleftarrows Sn_2(OH)_2{}^{2+} + 2H^+ \quad (3)$$

and

$$3Sn^{2+} + 4H_2O \rightleftarrows Sn_3(OH)_4{}^{2+} + 4H^+. \quad (4)$$

These reactions are viable due to the possibility of Sn^{2+} of increasing its coordination number, being the trimmer the dominant species [28]. Then, even without the addition of NH_4OH, polynuclear species of tin, dimmers and trimmers, are likely to occur. On the other hand, the aquo tin complex might also experience the hydrolysis reactions generalised in Eq. (5).

$$[Sn(OH_2)_N]^{2+} + hH_2O \rightleftarrows [Sn(OH)_h(OH_2)_{N-h}]^{+(2-h)} + hH_3O^+, \quad (5)$$

where N could be initially equal to 3 due to the structure of the original complex $[SnCl_2(OH_2)]\cdot H_2O$ [28]. Every reaction previously mentioned brings about a pH drop of the $SnCl_2$–H_2O system to an experimental value below 2.

When the addition of NH_4OH starts, an increase in the pH is seen in the potentiometric titration curve (AB region) due to the neutralization of the H^+ generated by the reactions cited above. Besides, ammonium hydroxide favours the hydrolysis of the tin–aquo complex and the formation of basic tin chlorides through the following reactions [29]:

$$[Sn(OH_2)_N]^{2+} + OH^- \rightarrow [Sn(OH)(OH_2)_{N-1}]^+ + H_2O \quad (6)$$

and

$$SnCl_2 + nNH_4OH \rightarrow Sn(OH)_nCl_{2-n} + nNH_4Cl. \quad (7)$$

The second region in the curve of Fig. 1 (BC region) does not show an important variation between pH 2.2 and 2.6 due to a rapid OH^- consumption. In this region, the formation of polynuclear species, such as $[Sn_2(OH)_2]^{2+}$, $[Sn_3(OH)_4]^{2+}$, $[SnO(OH)_2]^{2-}$ among others, may occur after the condensation of tin hydrolysed species.

Polynuclear tin complexes of the type oxi-hidroxo usually present a composition close to $3SnO\cdot H_2O$ so that XRD analyses reveal the presence of $Sn_6O_8H_4$ polyhedra that give rise to a pseudo-cubic structure. The basic unit would be an octahedron of SnO_6 with 8 oxygen atoms centred in the octahedron faces and the pseudo-cubes would be bonded through H-bonds causing a structural formula of $Sn_6O_8H_4$ [28]. This compound might arise from the condensation of $[Sn_3(OH)_4]^{2+}$ through the reaction in Eq. (8) favoured by the ammonium hydroxide addition:

$$2[Sn_3(OH)_4]^{2+} + 4OH^- \rightarrow Sn_6O_8H_4 + 4H_2O. \quad (8)$$

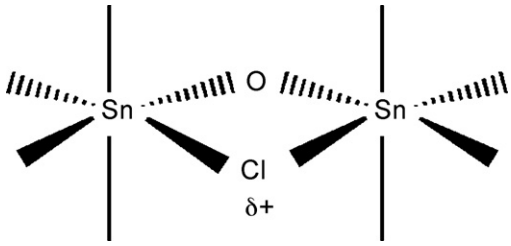

Fig. 2. Bridging chlorine structure.

Structures, such as that in Fig. 2, with bridging chlorines are also plausible. These structures, which have been reported to occur in other systems, allow indeed the formation of SnO_2 through an oxolation process [30].

The species and polynuclear structures formerly mentioned, might allow the conformation of the embryos and nuclei of the solid phase. According to the literature, the precipitation of SnO is expectable at pH 2; however, due to the presence of so many SnO-precursor species in the system (mainly tin oxi-hydroxides, $Sn_6O_8H_4$ and polynuclear Cl^- bridge complexes), the precipitation of this oxide would reasonably occur at a higher pH [26]. The instability of SnO must also be considered; it may turn into SnO_2 according to the following reaction that occurs slowly under normal conditions [27]:

$$SnO + H_2O \rightarrow SnO_2 + H_2. \quad (9)$$

In the BC region of the titration curve in Fig. 1, mainly polycondensation reactions (Eqs. (3), (4) and (8)) must occur. The resulting species would give rise to the embryos and nuclei of the solid phase in the suspension. The pH rise within the CD region stands for the growing of the nuclei accompanied by a reduction in the rate of formation of tin complexes and, consequently, of new nuclei.

Since Sn(II) is a B-type metal with a greater affinity to coordinate NH_3 species rather than H_2O, at pH values corresponding to the CD region, in which a great amount of NH_4OH is present in the system, the redissolution of the precipitate must be taken into account [29,30]:

$$Sn(OH)_nCl_{2-n} + nNH_4Cl + xNH_4OH \rightarrow SnCl_2\cdot(n+x)NH_3 + (n+x)H_2O. \quad (10)$$

Furthermore, due to the presence of Sn(IV) as a result of Eq. (9) and due to its high electropositivity, the formation of anions or polyanions of the type oxo or oxi-hidroxo is favoured by the solubility of this species in a basic medium [31]. The DE region in the titration curve, involving high pH values, may contain information on the redissolution of the solid phase and on the reactions of interchange of labile species that occur in the solvent-particles interphase.

The conductimetric titration curve in Fig. 1 that corresponds to the 0.3 M $SnCl_2$ system shows three regions and the usual profile of a weak acid–weak base titration. The first region, A′B′, represents the neutralization of the H^+ resulting from the reactions in Eqs. (1)–(5). The mobile species H^+ are being replaced by the $NH_4{}^+$ with a lower molar conductivity [32].

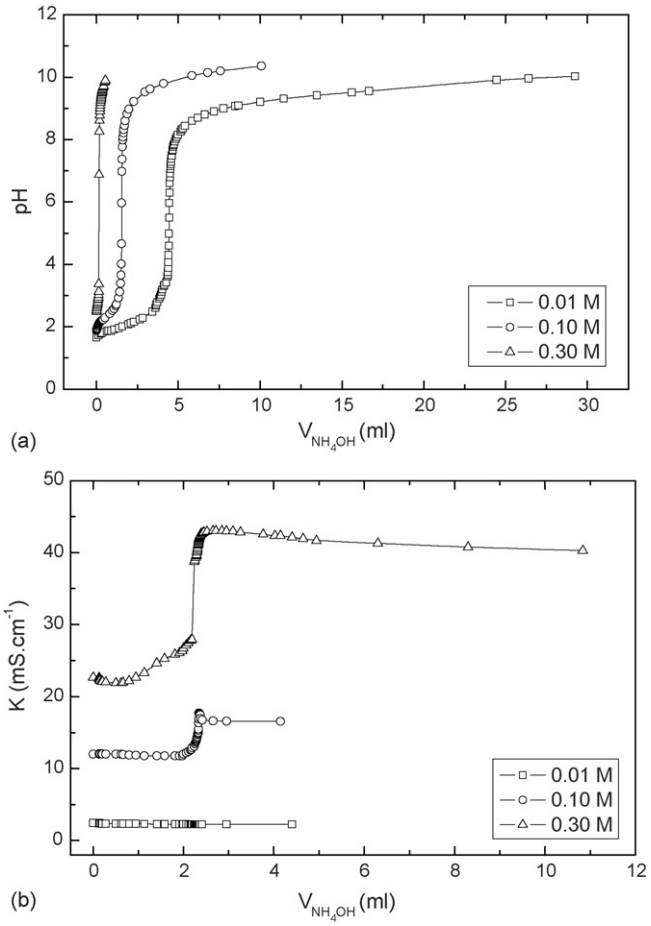

Fig. 3. (a) Potentiometric and (b) conductimetric titration curves of $SnCl_2$ aqueous dissolutions of different concentrations.

The curvature of the graph near the equivalence point is a consequence of water dissociation and of the presence of NH_4^+ and OH^- species [32,33].

The B′C′ region is constituted by small linear segments with varying slopes that would represent the titration of surface groups of weak acid–weak base nature. The intermediate tin compounds, and the nuclei of the solid phase, are formed in this region and the growing number of ions in solution and the excess of OH^- ions added are responsible for the increase in the conductivity of the system. The third region, C′D′, corresponds to the titration of the dissociated weak base added to the solution that contains an already formed solid phase and tin compounds that make the conductivity to vary slowly; moreover, at pH 9.2, the system NH_4^+/NH_3 acquires a buffer character where NH_3 is the dominant species.

Fig. 3 shows the potentiometric and conductimetric titration curves for different concentrations of the tin precursor. The profile of the curves is similar to that of the 0.3 M $SnCl_2$. In the B′C′ region, the three linear segments are clearly visible and must correspond to the titration of surface groups of weak acid nature. The non-linearity of the segments evidences the presence of polynuclear and polymeric groups of weak acid nature [33].

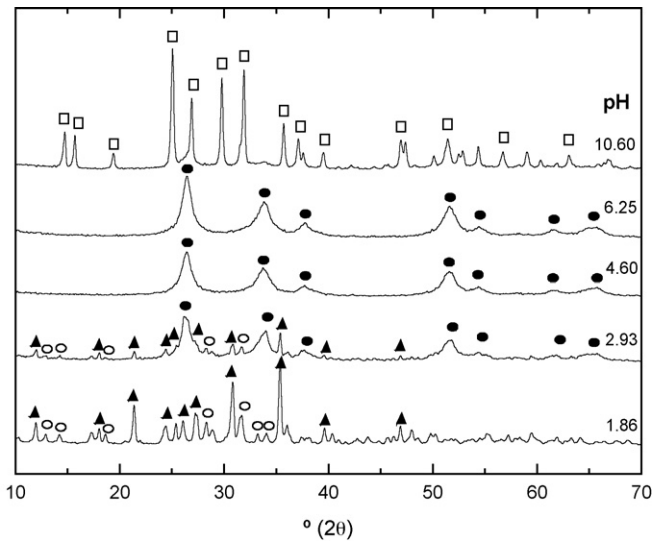

Fig. 4. XRD pattern of the solid formed at different pH values in the 0.3 M $SnCl_2$ dissolution: (▲) $Sn_3O(OH)_2Cl_2$; (◯) $SnCl(H_2O)_2SnCl_3(H_2O)$; (□) $Sn_6O_4(OH)_4$; (●) SnO_2.

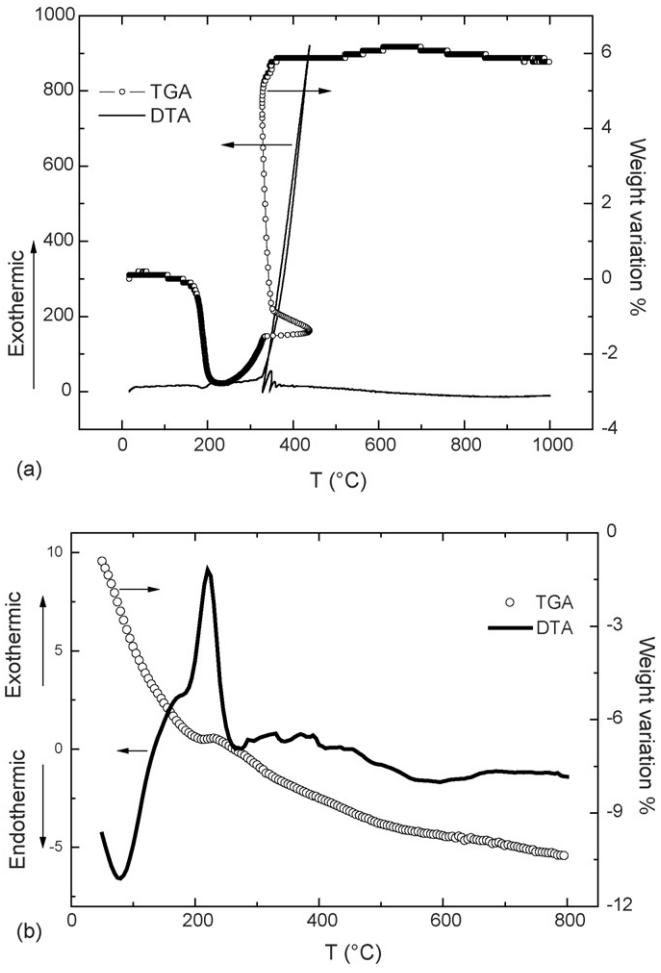

Fig. 5. DTA and TGA curves corresponding to the solid phase in the 0.3 M $SnCl_2$ aqueous dissolution at pH 6.25: (a) before and (b) after eliminating chlorine ions.

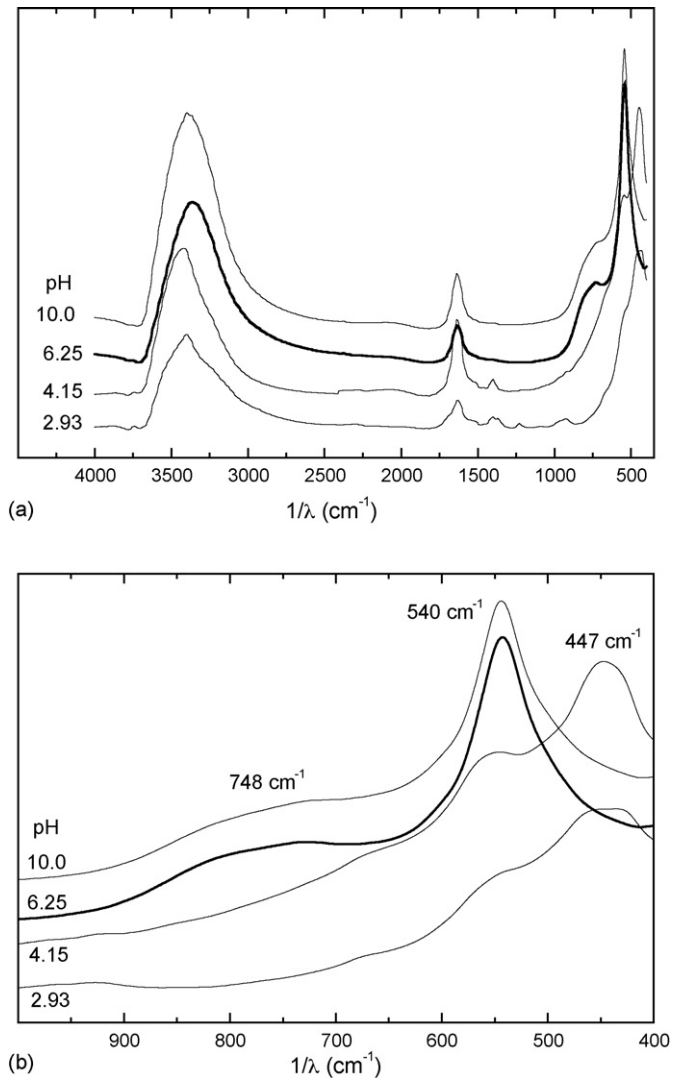

Fig. 6. (a) FTIR-absorption spectra of solid samples in the $SnCl_2$ aqueous dissolution at different pH values. (b) Magnification of the 1000–400 cm^{-1} region.

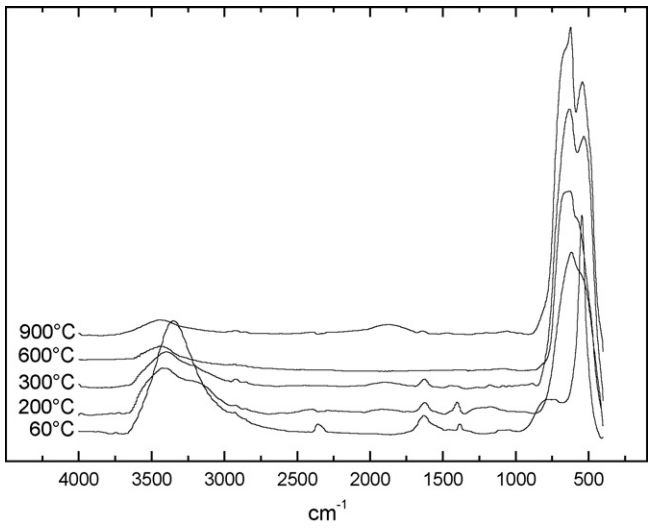

Fig. 7. FTIR-absorption spectra of the solid phase in the $SnCl_2$ aqueous dissolution at pH 6.25 after different thermal analyses.

3.2. Characterization of the solid phase present in the suspension

The solid phase present in the colloidal suspensions obtained after the NH_4OH addition until a desired pH value was reached, were characterized with X-rays diffraction, thermal analyses (DTA/TGA), FTIR spectroscopy and scanning electron microscopy.

3.2.1. X-rays diffraction

Fig. 4 shows the XRD powder patterns of the solid formed at different pH values in the 0.3 M $SnCl_2$ system. The main crystalline phases identified at pH values between 1.86 and 2.93 are abhurita ($Sn_3O(OH)_2Cl_2$; JCPDS 75-2328), hydrated tin chlorides ($SnCl(H_2O)_2SnCl_3(H_2O)$; JPDS 39-0314) and cassiterite (SnO_2; JCPDS 41-1445). These results allow to confirm the occurrence of the reactions that lead to the formation of basic chlorides and basic tin oxi-chlorides (Eqs. (1) and (7)) and the hydrolysis and polycondensation of the tin–aquo complex (Eqs. (2)–(6)) that lead to the formation of tin dioxide. Furthermore, the difficulty in the dissociation of the precursor is evident; even at this pH value the presence of tin chloride in the solid is recognised.

The pattern that resulted from the solid in the colloidal suspension at pH values between 4.6 and 6.25, shows the preponderance of a single phase: cassiterite (SnO_2; JCPDS 41-1445). However, the oxide is not very well crystallised as can be deduced from the breadth of the peaks. Therefore, the presence of other amorphous compounds in the solid, such as tin chlorides or basic oxi-chlorides cannot be totally neglected. The pattern that corresponds to the solid present at pH 10 reveals that the main crystalline phase present is a tin oxi-hydroxide ($Sn_6O_4(OH)_4$; JCPDS 84-2157).

From the previous results, with the addition of NH_4OH the following phase transformations can be considered. Starting with $SnCl(H_2O)_2$ and $SnCl_3(H_2O)$, the formation of $Sn_3O(OH)_2Cl_2$ would be favoured. It is originated from the $[Sn_3(OH)_4]^{2+}$ complex or from a similar one and is the main species in tin solutions at low pH values and also the precursor of the basic salts of Sn^{+2} that usually precipitate at pH 2 [34]. On

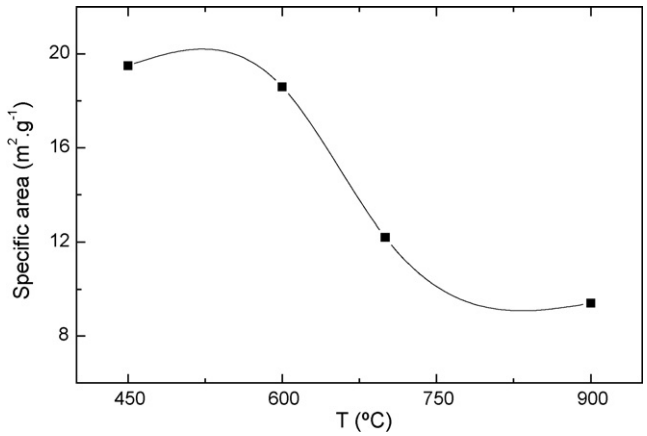

Fig. 8. Evolution of the surface area of the solid obtained from the 0.3 M $SnCl_2$ dissolution at pH 6.25.

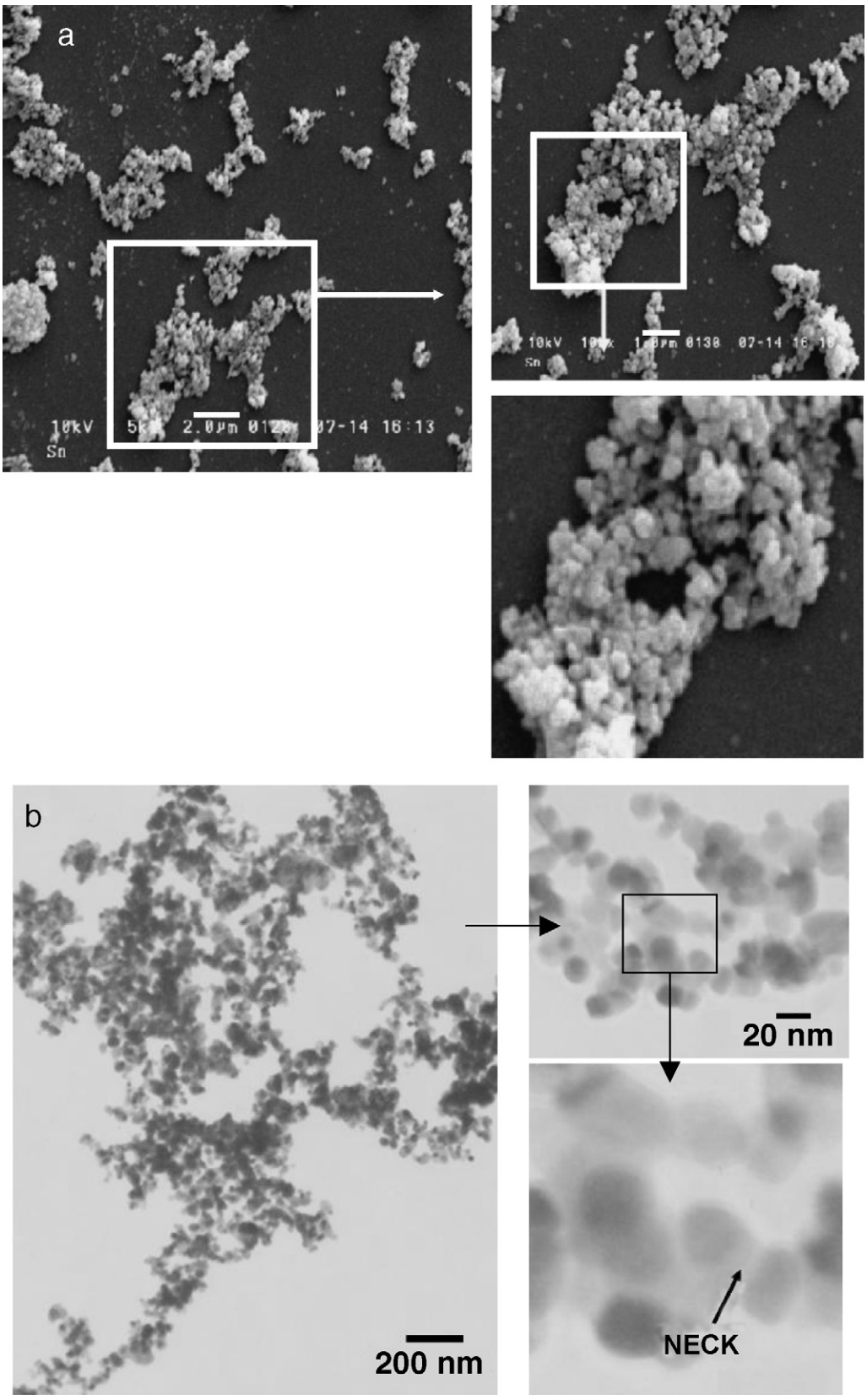

Fig. 9. (a) SEM and (b) TEM images obtained from the SnO_2 powder treated at 600 °C.

the other hand, when the concentration of OH^- is increased, the tin atom suffers a nucleophillic attack that helps to remove Cl^- ions and favours the formation of polynuclear tin oxi-hydroxide complexes with a composition close to $3SnO{\cdot}H_2O$ and with a structural formula of $Sn_6O_8H_4$. During the drying stage, this compound would turn into SnO that subsequently would give rise to SnO_2, the most stable phase seen in the XRD patterns of the suspensions at pH values between 4.6 and 6.25. Further additions of NH_4OH would turn the tin dioxide into an oxi-hydroxide given that the OH^- weakens the double bond between Sn and O.

3.2.2. Thermal analyses (DTA/TGA)

Fig. 5 shows the DTA and TGA curves corresponding to the solid obtained at pH 6.25; Fig. 5a belongs to the powder before the washing attempts to eliminate Cl^- species and Fig. 5b to the powder after the described washing process with diethylamine solution. In Fig. 5a, the weight loss that occurs at approximately 180 °C may be associated to the evaporation of structural water molecules. The oxidation of Sn^{2+} is seen as the increase in weight in Fig. 5a starting around 300–350 °C. Due to the heat released during the oxidation reaction, the temperature inside the furnace rapidly increased above the programmed temperature and a distortion appears in the TGA curve. Approximately, at 380 °C the constant weight condition is reached. The crystallization of cassiterite (SnO_2), and the transformation of tin compounds into SnO_2, is evidenced by the exothermic event that occurs near 350 °C. The TGA results confirm that a non-crystalline content of SnO is also present in the solid sample obtained at pH 6.25, even though in the XRD patterns only SnO_2 appears to be the prevailing phase.

Fig. 5b shows a continuous loss of weight during the whole temperature range studied. A constant weight region between 200 and 250 °C is observed, after which the OH^- loss due to the crystallization of SnO_2 determines a slow rate of weight loss. The endothermic signal before 100 °C in the DTA corresponds to the loss of water, whereas the exothermic signal at 220 °C might represent the rearrangements of the atoms in tin oxi-hydroxides that lead to the consolidation of the tin oxide structure and to its crystallization. The elimination of diethylamine still present in the system after the washing stage is evidenced by the signals around 350 °C. The variations observed in the base line of the DTA curve are ascribed to changes in the thermal conductivity due to the evolution of the sinterization process.

3.2.3. FTIR spectroscopy

Fig. 6 exhibits the FTIR spectra of solid samples at different pH values where the usual bands of stretching vibrations of the O–H bond between 3420 and 3400 cm^{-1} are recognised. In the region 1635–1629 cm^{-1}, the bending vibrations of H–O–H in water is evidenced while the bands around 1464 cm^{-1} corresponds to the stretching of the N–H bond in NH_4Cl or ammonium stannites and stannates. The signals between 1400 and 1368 cm^{-1} can be assigned to the N–O bond of the NO_3^- species present, whereas the band at 925 cm^{-1} may be originated by the N–H bond of the ammonia complexes formed in the surface of the particles. The bands below 900 cm^{-1} belong to Sn–O and Sn–OH bonds. At low pH values strong bands that are originated by the Sn–OH bond present in hydrated salts appear between 430 and 450 cm^{-1} and, bands around 550 cm^{-1}, correspond to the Sn–OH and Sn–O bonds of free oxi-hydroxides. Increasing the pH, the bands at 430 and 550 cm^{-1} disappear while the bands at 545, 750–780 and 630 cm^{-1} become stronger. The latter are associated to the vibration modes of the Sn–O–Sn bonds.

In Fig. 7, the FTIR spectra of the solid formed at pH 6.25 in the 0.3 M $SnCl_2$ system after different thermal treatments are shown. It is remarkable to note the disappearance of the bands at 1380 and 1458 cm^{-1} between 200 and 350 °C due to the removal of NO_3^- and NH_4^+ species. The intensity of the signals at 3400 and 545 cm^{-1} that correspond to the vibration of the O–H and Sn–OH bonds is also reduced because of water elimination reactions that lead to the development of Sn–O and Sn–O–Sn bonds which are evidenced by the bands at 700 and 630 cm^{-1} at temperatures above 300 °C. The results acquired confirm that at 600 °C mainly SnO_2 composes the solid.

3.2.4. Surface area measurements (BET)

The evolution of the specific surface of the SnO_2 particles obtained at pH 6.25 from the 0.3 M $SnCl_2$ system is shown in Fig. 8. It can be seen that this property remains almost constant at 19.5 $m^2\,g^{-1}$ until 600 °C. A rapid reduction in the specific area is registered after a further increase in temperature; the particles coalesce due to the activation of transport mechanisms and solid-state diffusion.

3.2.5. Electron microscopies (SEM, TEM)

Fig. 9a corresponds to the micrograph obtained through SEM of the SnO_2 powder calcinated at 600 °C. It shows the presence of nanometric particles with average size below 200 nm agglomerated in sponge-type arrays of around 5 μm. On the other hand, it could be determined through TEM (Fig. 9b) that the sample consists in a very homogeneous powder with an average particle size of 20–60 nm. Aided by temperature and also by their intrinsic high surface energy and reactivity confirmed by the surface area measurements, the particles are seen to form necks between each other.

4. Conclusions

Through the controlled precipitation method the synthesis of SnO_2 with defined properties, such as particle size and shape and with a high reproducibility was achieved. The optimum pH value that yielded the desired product, cassiterite, as the major phase was determined to be 6.25 on the basis of XRD analyses.

The tin complexes and compounds that aroused in the system were described in detail through hydrolysis and condensation reactions. At low pH values, the formation of basic chlorides or oxi-chlorides is favoured whereas at high pH values the tin oxi-hidroxy species are the main species present. The evolution of the most important functional groups during the Cl^- removal process, as well as during thermal treatment of the samples,

was explained in view of the results obtained with FTIR. These results are in well agreement with those obtained with XRD.

As concluded from the thermal analyses, the main events that take place at temperatures above 350 °C that eventually lead to the formation of SnO_2 are the removal of volatile species that resisted the washing process and the consolidation of the solid phase due to dehydration reactions.

Additionally, the obtained cassiterite is highly reactive and its surface area shows a decreasing trend at temperatures higher than 600 °C. Even at this temperature, the sample showed a high reactivity. Interestingly, the powder prepared through this route of synthesis presents a nanometric-scale particle size (<50 nm) with a surface area ($19\,m^2\,g^{-1}$) greater than that of usual SnO_2 powders ($5\,m^2\,g^{-1}$).

Acknowledgements

The authors express their thanks to the Project VIII.13 PROALERTA-CyTED, to Program CIAM, to CONICET (Argentina) and to COLCIENCIAS No. 1103-14-17900 (Colombia) for the financial support. Thanks are also given to Patricia Mosquera from the Laboratory of Microscopy of the UNICAUCA, Popayán.

References

[1] K.J. Klanbunde, Nanoscale Materials in Chemistry, John Wiley & Sons, Inc., New York, 2001.
[2] A.S. Edelstein, R.C. Cammarata (Eds.), Nanomaterials: Synthesis, Properties and Applications. Series in Micro and Nanoscience and Technology, Institute of Physics Publishing Ltd., Bristol, 2002.
[3] F.F. Lange, J. Am. Ceram. Soc. 72 (1989) 3.
[4] W. Luan, L. Gao, J. Guo, Nanostruct. Mater. 10 (1998) 1119.
[5] E. Matijevic, Chem. Mater. 5 (1993) 412.
[6] E. Matijevic, Langmuir 2 (1986) 12.
[7] J.M. Jorzebsk, J.P. Marton, J. Electrochem. Soc. 129 (1976) 299C.
[8] N.S. Baik, G. Sakai, N. Miura, N. Jamazoe, J. Am. Ceram. Soc. 83 (2000) 2983.
[9] P. Olivi, E.C.P. Souza, E. Longo, J.A. Varela, L.O.S. Bulhões, J. Electrochem. Soc. 140 (1993) 81.
[10] K.L. Chopra, S. Major, D.K. Pandya, Thin solids films 102 (1983) 1.
[11] T. Tagawa, S. Kataoka, T. Hattori, Y. Murakami, Appl. Catal. 4 (1994) 1.
[12] P.W. Park, H.H. Kung, D.W. Kim, M.C. Kung, J. Catal. 184 (1999) 440.
[13] S.A. Pianaro, P.R. Bueno, E. Longo, J.A. Varela, J. Mater. Sci. Lett. 14 (1995) 692.
[14] P.R. Bueno, M.R. Cássia-Santos, E.R. Leite, E. Longo, J. Bisquert, G. Garcia-Belmonte, F. Fabregat-Santiago, J. Appl. Phys. 88 (2000) 6545.
[15] A.C. Bose, D. Kalpana, P. Thangadurai, S. Ramasamy, J. Power Sources 107 (2002) 138.
[16] N. Segent, P. Gelin, L. Perrier, H. Praliaud, G. Thomas, Sens. Actuators B 84 (2002) 176.
[17] M. Ristic, M. Ivanda, S. Popovic, S. Music, J. Non-Cryst. Solids 303 (2002) 270.
[18] L. Broussous, C.V. Santilli, S.H. Pulcinelli, A.F. Craievich, J. Phys. Chem. B 106 (2002) 2885.
[19] J. Zhang, L. Gao, J. Solid State Chem. 177 (2004) 1425.
[20] Z.X. Deng, C. Wang, Y.D. Li, J. Am. Ceram. Soc. 85 (2002) 2837.
[21] E.R. Leite, J.W. Gomez, M.M. Oliveira, E.J.H. Lee, E. Longo, J.A. Varela, C.A. Paskocimas, T.M. Boschi, F. Lanciotti, P.S. Pizani, P.C. Soares, J. Nanosci. Nanotechnol. 2 (2002) 125.
[22] E.R. Leite, A.P. Maciel, I.T. Weber, P.N.L. Filho, E. Longo, C.O.P. Santos, C.A. Paskocimas, Y. Maniette, W.H. Schreiner, Adv. Mater. 14 (2002) 905.
[23] D.E. Niesz, R.B. Bennett, M.J. Snyder, Am. Ceram. Soc. Bull. 51 (1972) 677.
[24] A. Roosen, H. Hausener, Adv. Ceram. Mater. 3 (1988) 131.
[25] O. Vasylkiv, Y. Sakka, J. Am. Ceram. Soc. 84 (2001) 2489.
[26] F. Burriel, F. Conde, S. Arribas, J. Hernandez, Química Anlítica Cualitativa, Paraninfo (Ed.), 1994.
[27] C.F. Baes, R.E. Mesiner, The Hydrolysis of Cations, Wiley-Interscience, John Wiley & Sons, Inc., New York, 1976.
[28] N.N. Greenwood, A. Earnshaw, Chemistry of the Elements, Butter-Worth-Heinemann Ltd., 1995.
[29] A. Ortiz, M. Mendoza, J.E. Rodríguez-Páez, Mater. Res. 4 (2001) 265.
[30] W. Stumm, J.J. Morgan, Aquatic Chemistry, John Wiley & Sons Ltd., New York, 1996.
[31] J.-P. Jolivet, Metal oxide Chemistry and Synthesis, from Solution to Solid State, John Wiley & Sons Ltd., New York, 2000.
[32] D.R. Crow, Principles and Applications of Electrochemistry, Blakie Academic & Professional, 1994.
[33] A. Homola, R.O. James, J. Colloid Interface Sci. 59 (1977) 123.
[34] P.J. Smith, Chemistry of Tin, Blackie Academic & Professional, 1998.